

Investigation on Erosion of Continuous Bending Pipes in Different Directions

Bingcheng Li, Wei Li, Min Zeng*, Qiuwang Wang

School of Energy and Power Engineering, Xi'an Jiaotong University, Xi'an, 710049, P. R. China
 zengmin@mail.xjtu.edu.cn

With the increasing demand for natural gas in the world, ensuring the safety and stability of pipeline transportation of natural gas has become an important subject. Compared with the studies focused on the erosion of single bend, T-pipe, and U-pipe, the studies on the continuous bend in different directions are scarce. In this paper, the model is characterized by three straight pipes with the same length and directions along the Z, Y, and X axes of the Cartesian coordinate system. The numerical simulation of gas-solid two-phase flow under different gas to solid mass ratios in the continuous bent pipeline is carried out by selecting the Oka erosion model. The results indicate that the velocity distribution of the second bend is different from that of the first bend. With the change of flow deflection angle and the accumulation of the centrifugal force, the shape of the velocity contours in the second bend turns from "basin" into a "comma" and the velocity experiences a process including rapid increase, slow decrease, gradual increase, and steep decrease. When the flow rate is 12.5 m/s, the maximum speed of the second bend is about 5 % greater than that of the first bend. Instead of a "straight-line" shape in the erosion area of the first bend, the second presents a "feather" shape. As the flow rate increases gradually, the shape characteristics of the "feather" erosion zone change from "short and dense" to "long and loose". Besides, the maximum erosion rate of the second bend is greater than that of the first even about 1.52 times. Finally, according to the simulation results, the protection suggestion of the continuous elbow is given.

1. Introduction

Pipeline transportation has many advantages such as a large amount of transportation, less occupation, safety, and reliability. However, natural gas in the pipeline is often mixed with solid particles, which causes erosion and wear of the pipe especially at the bend including pipeline leakage, equipment scrapped, etc., resulting in huge economic losses.

Most of the previous research including the papers mentioned considered single elbow, U-pipe, and T-pipe. Sedrez et al. (2019) selected Euler-Lagrange and other methods to perform numerical simulations to study the erosion rates regulation of particles with different sizes and concentrations at a single bend. Kannojiya et al. (2018) used CFD-CFX to investigate the erosion rates of a single elbow with different particle sizes and concentrations. Elemuren et al. (2018) analysed that the reason why the erosion-corrosion rate of the elbow increases with the flow velocity by studying the flow velocity on the erosion damage of a single steel bend. Asgharpour et al. (2020) proposed an erosion strength and an erosion law of gas-sand and gas-liquid-sand on U-pipe. Zhu and Qi (2019) used the DPM erosion prediction model to study the erosion behaviour of liquid-solid two-phase flow in U-pipe. Jamwal (2020) carried out a numerical simulation on T-pipe and study the related erosion influence factors. Elkarii et al. (2020) studied the dynamic behaviour of phosphate flow in a pipe under controlled isothermal conditions. Xu et al. (2018) investigated the erosion characteristics of gas-solid two-phase flow pipelines, including different solid content, throttle valve opening.

Due to the restriction of topographic factors and the need for pipeline installation, the continuous bent pipeline composed of three vertical pipes and two bends is also common in the natural gas pipeline network. However, the research on erosion protection of this type of pipeline is not sufficient. It is of no difficulty to find from the existing research that the degree and area of erosion may vary, even if the same fluid flows through different types of pipelines. Similarly, different multiphase flow media will produce different results on the erosion of pipelines with the same structure. As the total length of natural gas pipeline transportation increases, it is

necessary to maintain the safety of transportation. In this paper, a numerical model of continuous bending pipe along three mutually perpendicular directions is established and suitable mathematical equations for the structure are selected. The ANSYS Fluent software (ANSYS, 2018) is used, and the Oka erosion model (Oka and Yoshida, 2005) is adopted to study the particle flow.

2. Mathematical models

It is assumed that the fluid is a continuous medium, particles continuously fill the whole space and the mass of the fluid system does not change with time. Eq(1) is a continuity equation in integral form (Kong, 2003). V is the volume of the fluid, N is the mass of the fluid system, ρ is the fluid density, v_n is the velocity component in the normal direction outside the control plane, CV represents the control volume and CS represents the control surface.

$$\frac{\partial}{\partial t} \iiint_{CV} \rho dV + \iint_{CS} \rho v_n dA = 0 \quad (1)$$

During the simulation process, the time changing rate of a certain physical quantity in the fluid system composed of gas and gravel gas-solid two-phase flow in the pipeline is equal to the sum of the changing rate of the physical quantity and the net flow through the control surface, as shown in Eq(2).

$$\frac{dN}{dt} = \frac{\partial}{\partial t} \iiint_{CV} \eta \rho dV + \iint_{CS} \eta \rho v_n dA \quad (2)$$

In Eq(3), \vec{f} is the mass force acting on the unit mass fluid, and \vec{p}_n is the surface stress acting on the infinitesimal surface dA .

$$\frac{\partial}{\partial t} \iiint_{CV} \rho \vec{v} dV + \iint_{CS} \rho v_n \vec{v} dA = \iiint_{CV} \rho \vec{f} dV + \iint_{CS} \vec{p}_n dA \quad (3)$$

The force balance equation of eroding sand and gravel particles can be simply described as the inertia of the particle being equal to the resultant force acting on it. Fluent software predicts the motion trajectory by force balance on discrete phase particles, and its equation can be expressed as Eq(4) (Amovilli et al., 2000).

$$m_p \frac{d\vec{v}_p}{dt} = m_p \frac{\vec{v} - \vec{v}_p}{\tau_p} + m_p \frac{\vec{g}(\rho_p - \rho)}{\rho_p} + \vec{F} \quad (4)$$

In Eq(4), m_p is the particle mass, \vec{v}_p is the particle velocity, ρ and ρ_p are the continuous phase density and particle density, and τ_p is the particle relaxation time (Gosman and Loannides, 1983). What's more, \vec{F} is the additional force acting on the particle when the fluid around the particle accelerates as Eq(5). C_{ad} is the virtual mass coefficient.

$$\vec{F} = C_{ad} m_p \frac{\rho}{\rho_p} (\vec{v}_p \nabla \vec{v} - \frac{d\vec{v}_p}{dt}) \quad (5)$$

The k- ϵ realizable model is selected since it performs well in flow separation and complex secondary flows. In order to predict the erosion damage caused by the impact of solid particles by combining the characteristics of the computational domain model and considering the mechanical properties of materials in the simulation process, the Oka erosion model shown in Eq(6) is selected.

$$E_{ero} = E_{90} \left(\frac{V}{V_{ref}} \right)^{k_2} \left(\frac{d}{d_{ref}} \right)^{k_3} f(a) \quad (6)$$

In Eq(6), E_{90} is the reference erosion rate when the impact angle is 90° , V_{ref} is the reference speed and d_{ref} is the reference particle diameter. k_2 and k_3 are the velocity index and the particle size index. $f(a)$ is the function of impact angle.

$$f(a) = (\sin a)^{n_1} (1 + H_V (1 - \sin a))^{n_2} \quad (7)$$

In Eq(7), a is wall impact angle and H_V is Vickers hardness of wall material, n_1 and n_2 are both angle function constants.

3. Computational domain models

The geometric model established in this paper is completed in SolidWorks 2021 SP1.0 and the characteristics of the model are that the length of three straight pipes is set at 5 m and the directions are along the Z-axis, Y-axis and X-axis of the Cartesian coordinate system. The wall thickness is 18 mm and the inner diameter of the natural gas pipeline is 1.08 m. The joints are connected by an elbow with an inner arc radius of 1m to form a continuous bent pipe model with different directions. The hexahedral mesh is formed by the method of scanning. In order to ensure the calculation accuracy, save the calculation cost, and make efficient numerical simulation realisable, local compaction is carried out at two elbow parts as shown in Figure 1a and the mesh quality is shown in Figure 1b.

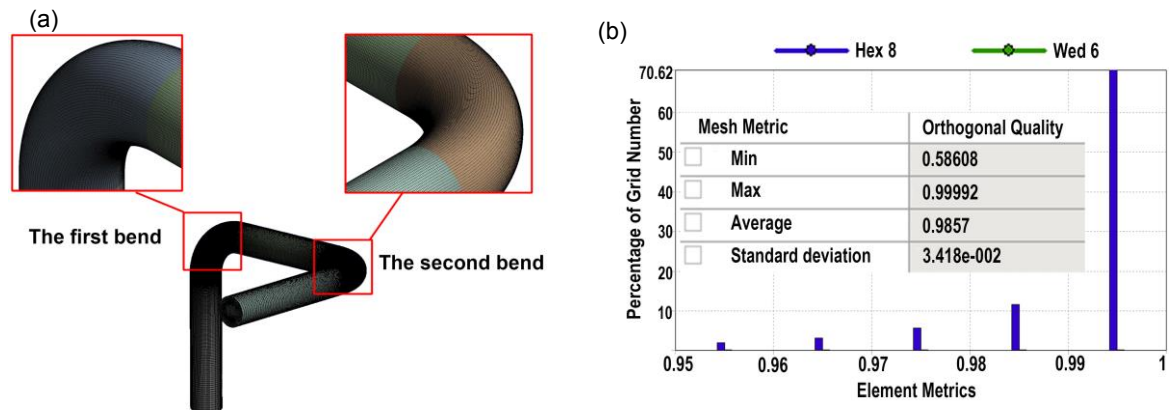


Figure 1: Geometric mesh model with local compaction (a) and mesh quality (b)

In terms of grid independence verification, this paper sets the different number of grids and studies the influence of grid numbers on simulation results by comparing the change of inlet and outlet pressure difference. The results clearly demonstrate that with the increase of mesh number, the pressure difference between inlet and outlet ΔP tends to be the same as shown in Table 1. In order to consider the accuracy of the simulation results and the economy of the calculation amount, the mesh number of Mesh 3 is selected as 1.3914 M.

Table 1: Grid independence analysis

Category	Quantity (M)	ΔP (Pa)
Mesh 1	0.6281	57.279
Mesh 2	0.9533	57.304
Mesh 3	1.3914	57.315
Mesh 4	2.0312	57.317

4. Results and discussion

The movement of gas-solid two-phase flow directly affects the erosion degree of the pipeline. The direction of gas-solid two-phase flow at the entrance is along the pipeline and the fluid flows evenly in the calculation domain of the selected continuous bent pipeline with the flow rate at 12.5 m/s. The angle of the bend position of the continuous bent pipe is selected. As shown in Figure 2a and Figure 2b, the radial direction of the pipe section circle is used as an auxiliary line to extract fluid velocity data to draw the line chart.

Figure 2a and Figure 3a show that when the first elbow is located in the region from 15° to 60° , the velocity contours of the fluid from inlet to outlet of the first elbow present a stratified phenomenon. The high-speed area is distributed inside the elbow while the low-speed area is located outside the elbow. The two-phase flow has a direct impact on the outside of the first bend and an indirect impact on the inside of the bend, compressing the outer side of the first elbow more than the inner side under the action of centrifugal force. Consequently, the outer side pressure is higher but the inner side pressure is lower. According to the Bernoulli equation, the velocity distribution is just opposite to the pressure distribution, and the high-speed region is distributed inside the bend. In the $75^\circ \sim 90^\circ$ region, the velocity contours at the first bend change gradually and a low-speed zone appears inside the bend. With the increase of the flow deflection angle, the area of the low-speed zone becomes larger because of local secondary flows. The flow separation phenomenon becomes increasingly obvious. The high-speed area originally inside the bend gradually moves to the outside. As the deflection angle is 85° , the velocity in other areas tends to be uniform except for the low-speed area.

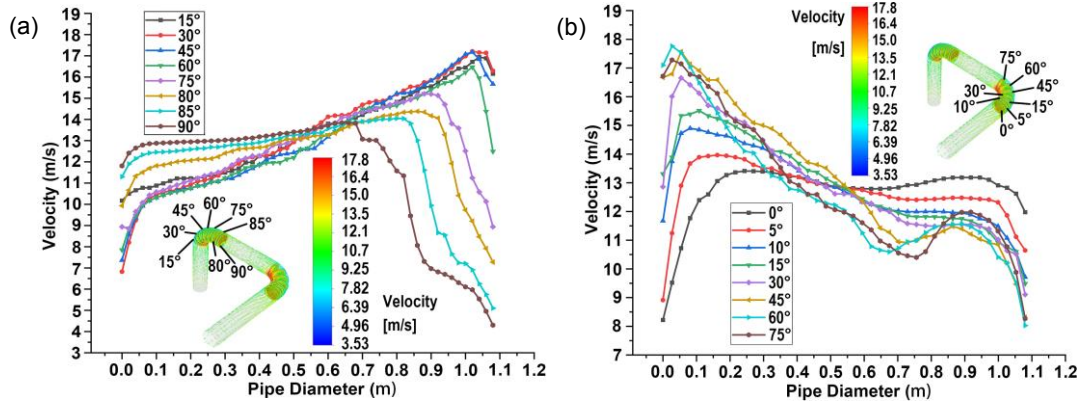


Figure 2: Section segmentation of the deflection angle at the (a) first bend, (b) second bend and velocity line diagram at the split section

Generally, when the two-phase fluid flows through the first bend, the peak velocity reaches 17.8 m/s at the flow deflection angle of about 30° and is located inside the bend. Figure 2b and Figure 3b reveal that the velocity distribution of the second bend is significantly different from that of the first bend. The inner side of the second bend from 75° to 30° is the high-speed region. An obvious low-speed zone is formed in the central area of the second bend and the shape of the velocity contour is similar to a "basin", i.e., the velocity around the area is high but the middle area is low. Along the decreasing direction of the flow deflection angle, the central low-speed area of the "basin" shape velocity distribution gradually moves to the left side with the accumulation of centrifugal force. Under the dual influence of the flow in the first and the second elbow, the velocity contour with the shape of "comma" is formed when the flow deflection angle at the second elbow is 45°. The "comma" shape gradually disappears and the velocity distribution becomes uniform in 30° ~ 0°. Although the degree of separation is less obvious than that of the first bend, it shows a new tendency to deviate slightly to the bottom right in 5° ~ 0°. As the gas-solid two-phase fluid flows through the second elbow, the peak velocity reaches 17.8 m/s and occurs at 60°. The reason for the rapid increase and steep decrease is that there is a velocity boundary layer at the contact point between the fluid and the wall surface due to the viscosity. The flow state of the fluid changes when it passes through the first elbow and the flow at the second bend will be affected by the first. Under the action of a secondary flow induced by centrifugal force, the velocity distribution curve appears distorted on the inside and forms a phenomenon that the velocity curve changes slowly.

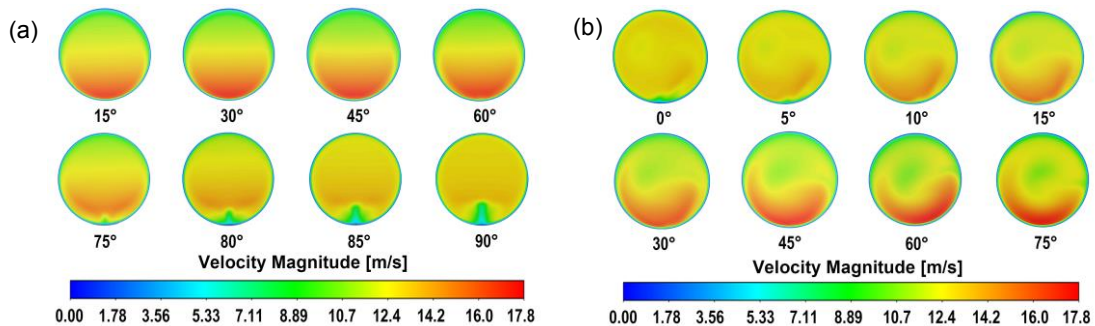


Figure 3: Velocity distribution contours at the (a) first bend, (b) second bend

The solid particles close to the top of the pipe begin to move towards the outside of the second elbow as shown in Figure 4 and two phenomena are generally observed. Firstly, the solid particles in the gas-solid two-phase flow just pass through the second elbow and are thrown to the outside of the elbow with the flow rate lower than 30 m/s. On account of the collision and extrusion between particles and the pipe wall, and the interaction among particles, some particles turn to the inner wall of the elbow and the trajectory of particles is complex. Secondly, as the flow rate is more than 30 m/s, the flowing particles are tightly pressed on and bounced off the wall. With the increase of the two-phase flow velocity, the concentration distribution of particulate matter at the first bend disperses from the spotty pattern at 10 m/s and then forms an O-shape concentrated distribution area at 20 m/s and 30 m/s as shown in Figure 5. When the flow rate increases to 40 m/s and 50 m/s, the concentrated distribution area of particles gradually gathers to the central axis outside the first elbow. Differently, the contour

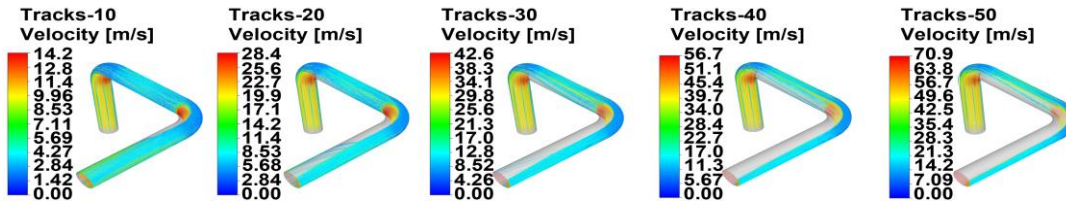


Figure 4: Trajectory and velocity distribution of particles at five flow rates from 10 m/s to 50 m/s

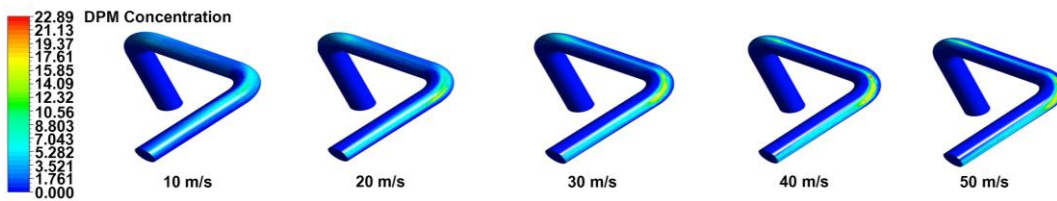


Figure 5: Distribution of particulate matter concentration at the wall surface of a continuous bent pipe

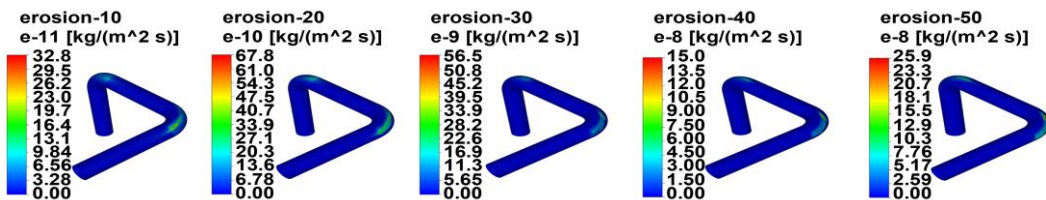


Figure 6: Erosion on continuous bent pipe with Oka model from 10 m/s to 50 m/s

at the second bend appears as a ribbon and the value of DPM concentration is more than $5.2820 \times 10^{-4} \text{ kg/m}^3$ and the maximum value is $2.289 \times 10^{-3} \text{ kg/m}^3$ from the second bend to the third straight pipe. Figure 6 explicitly shows the maximum erosion rate increases from $3.28 \times 10^{-10} \text{ kg}/(\text{m}^2\text{s})$ at 10 m/s to $2.59 \times 10^{-7} \text{ kg}/(\text{m}^2\text{s})$ at 50 m/s and the erosion rate of the second bend is greater than that of the first one. The erosion position of the first elbow is mainly located in the central area of the outer wall and relatively concentrated in general, presenting as O-shape at low speed or straight-line shape at high speed. The erosion position of the second elbow is lateral to the upper part of the second elbow, showing the shape of a feather. Generally, the lower speed is, the smaller and denser “feather” forms. The higher speed is, the bigger and looser “feather” appears. As the velocity of gas-solid two-phase flow is less than 20 m/s, the erosion of the second elbow is greatly affected by the first elbow. The stronger the solid particle follows the fluid, the greater the drag force exerted by the fluid on the particle.

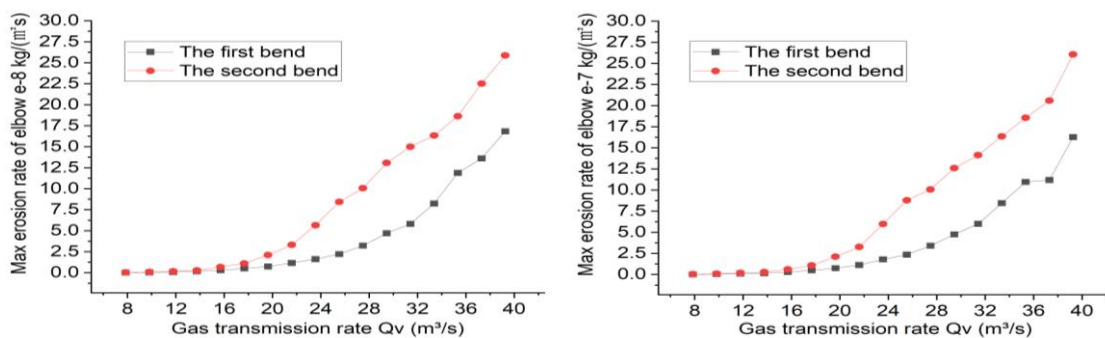


Figure 7: The curve of maximum erosion rate as a function of gas transport with gas to solid mass ratio at 56257.62 (a), at 5625.762 (b)

With the increase of gas transmission volume, the velocity of gas-solid two-phase flow increases gradually as shown in Figure 7a and Figure 7b. The maximum erosion rate of the pipeline gradually increases and the overall erosion curve increases quasi exponentially in the range. The maximum erosion rate of the second bend is greater than that of the first bend. When the gas volume is less than $12 \text{ m}^3/\text{s}$, the erosion rate of gas-solid two-phase flow on the pipeline is almost zero. As the gas volume is greater than $22 \text{ m}^3/\text{s}$, the erosion rate will increase with a larger span for each unit of gas volume increase. In addition, when the gas-solid mass ratio is

reduced to 1/10, the overall trend of the maximum erosion rates of the two bends is the same, and the corresponding maximum erosion rates are also about 1/10.

5. Conclusions

The erosion phenomenon of the continuous bends located in three mutually vertical directions is simulated through ANSYS Fluent. The principal conclusions follow. The erosion degree of the second bend is greater than that of the first one and the erosion position is different. The maximum erosion rate increases from 3.28×10^{-10} kg/(m²s) at 10 m/s to 2.59×10^{-7} kg/(m²s) at 50 m/s. The erosion area of the first bend is mainly located in the central area of the outer wall and is relatively concentrated in general, presenting as O-shape at low speed or straight-line shape at high speed. The erosion area of the second elbow shows a "feather" shape. As the flow rate increased, the "feather" erosion zone in the second bend change from "short and dense" to "long and loose". The velocity distribution of the two bends presents a distinct variation. The velocity separation phenomenon gradually increases along the direction of increasing deflection angle, and the velocity distribution in the first bend is significantly distorted. The flow trajectories of gas-solid two-phase fluid vary greatly. When the flow rate is less than 30 m/s, some particles no longer flow close to the outside of the elbow but turn to the inner wall of the elbow. When the flow rate is greater than 30 m/s, the centrifugal force increases and almost all the flowing particles are tightly pressed on the outside of the elbow, and a local particle-free erosion area is formed inside the tube. In practical engineering applications, an idea to determine two critical reference values by numerical simulation can be regarded as a reference. Provided that the gas flow is controlled below the first critical reference value, the erosion rate is negligible, and long-term safe transportations can be guaranteed. The gas flow is supposed to be kept below the second critical reference value as much as possible. According to the trajectory image and erosion contours, the outer side of the first elbow and the "feather" erosion area of the second elbow is expected to be heavily protected. Aiming at the sidewall where solid particles collide and rub, the anti-erosion performances of the material at this position ought to be considered in the design process of the pipeline. Even unilateral wall thickening can be considered.

In this paper, the research of continuous elbow erosion is limited by two variables. In the future, the influence of the various distance between the two bends and the rules of particle size, roundness, and other factors on the erosion of the elbow will be further explored.

References

- Amovilli C., March N. H., Gal T., Nagy A., 2000, Force-balance and differential equation for the ground-state electron density in atoms and molecules, *International Journal of Quantum Chemistry* 77(4): 716-720.
- ANSYS, 2018, ANSYS Fluent User's Guide, Release 19.0. ANSYS, Canonsburg, PA.
- Asgharpour A., Zahedi P., Khanouki H. A., Shirazi S. A., McLaury B. S., 2020, Experimental Investigation of Solid Particle Erosion in Successive Elbows in Gas Dominated Flows, *Journal of Fluids Engineering-Transactions of the Asme* 142(6).
- Elemuren R., Evitts R., Oguocha I., Kennell G., Gerspacher R., Odeshi A., 2018, Slurry erosion-corrosion of 90 degrees AISI 1018 steel elbow in saturated potash brine containing abrasive silica particles, *Wear* 410: 149-155.
- Elkarii M., Bouallou C., Ratnani A., 2020, Towards Modelling a Diphasic Flow Using the CFD Technique to Achieve a Digital Twin of a Phosphate Slurry Piping Process, *Chemical Engineering Transactions*, 81, 757-762.
- Gosman A. D., Loannides E., 1983, Aspects of Computer-Simulation of Liquid-Fueled Combustors, *Journal of Energy* 7(6): 482-490.
- Jamwal A. S., 2020, Comparative Study of Particulate Erosion Phenomena Between Elbow and Target Tee in Pipe Flow, *Trends in Manufacturing Processes, Icfmm 2018*: 153-159.
- Kannojiya V., Deshwal M., Deshwal D., 2018, Numerical Analysis of Solid Particle Erosion in Pipe Elbow, *Materials Today-Proceedings* 5(2): 5021-5030.
- Kong, Long (Ed.), 2003, *Fluid Mechanics II[M]*. Beijing: Higher Education Press.
- Oka Y. I., Yoshida T., 2005, Practical estimation of erosion damage caused by solid particle impact - Part 2: Mechanical properties of materials directly associated with erosion damage, *Wear* 259(1-6): 102-109.
- Sedrez T. A., Shirazi S. A., Rajkumar Y. R., Sambath K., Subramani H. J., 2019, Experiments and CFD simulations of erosion of a 90 degrees elbow in liquid-dominated liquid-solid and dispersed-bubble-solid flows, *Wear* 426: 570-580.
- Xu, J. Y., Lian, Z. H., Hu, J., Luo, M., 2018, Prediction of the Maximum Erosion Rate of Gas-Solid Two-Phase Flow Pipelines, *Energies* 11(10).
- Zhu, H. J., Qi, Y. H., 2019, Numerical investigation of flow erosion of sand-laden oil flow in a U-bend, *Process Safety and Environmental Protection* 131: 16-27.